IEEE Access
Multidisciplinary | Rapid Review | Open Access Journal

Received February 18, 2021, accepted March 1, 2021, date of publication March 10, 2021, date of current version March 30, 2021.

Digital Object Identifier 10.1109/ACCESS.2021.3065497

The Radiation Effect on Low Noise Amplifier Implemented in the Space-Aerial–Terrestrial Integrated 5G Networks

ABDOURAOUF SAID YOUSSOUF, MOHAMED HADI HABAEBI, (Senior Member, IEEE), AND NURUL FADZLIN HASBULLAH

Department of Electrical and Computer Engineering, International Islamic University, Kuala Lumpur 53100, Malaysia

Corresponding author: Nurul Fadzlin Hasbullah (nfadzlinh@iium.edu.my)

This work was supported by the Ministry of Higher Education Malaysia through the Research Grant under Grant FRGS 19-053-0661.

ABSTRACT This paper provides the details of a study on the effects of electron irradiation on two Low Noise Amplifiers (LNA), the Gallium-Arsenide (GaAs) pseudomorphic high electron mobility transistor (pHEMT) based and the Silicon-Germanium (SiGe) Heterojunction Bipolar Transistor (HBT)-based. Previous studies have shown that the properties of GaAs and SiGe HBT's are very tolerant of gamma, neutron, and proton irradiation without additional radiation hardening. Nowadays, commercials on the shelves (COTS) LNAs have been used in CubeSat space communication systems which may be connected to other communication networks for the implementation of the space-aerial- terrestrial integrated 5G network (SATIN) systems projects, for satellites, launched into Low and Medium Earth Orbits. Previous studies suggest that the electron radiation in space may degrade the LNAs' performance and might even lead to its failure. Located at the front end of the communication receiver system, this paper conducted such investigation to evaluate the performance under the radiation of the GaAs and SiGe LNAs considering the physics of the technology of each LNA, respectively. The results indicate that both SiGe and GaAs technologies are affected after electron irradiation. As a result, this degradation of the LNAs' performance affected the communications system performance of the inter-satellite radio link. After the assessment of the quality performance of the communication link at the system level, it has been found that the inter-satellite space link will be at risk under high space radiation dose and the link BER degrades proportionally to the radiation dose level.

INDEX TERMS Degradation, electron irradiation, gallium arsenide, inter-satellite link, low noise amplifier, silicon germanium, 5G.

I. INTRODUCTION

To improve performance and reduce the cost of the communication systems, academia and industry are active in the discovery of adequate solutions. With the introduction of the fifth-generation (5G), users are expecting reliable broadband services everywhere at a reasonable cost. However, the terrestrial network alone may not able to achieve quality service availability at any time and place, especially in a harsh environment such as oceans and mountains [1].

Therefore, the proposition comes to develop a non-terrestrial integrated 5G system [2]. Both satellite industry and communication start to work on this new paradigm to integrate the space, aerial and terrestrial networks to form the three-dimensional of 5G [3], [4].

The associate editor coordinating the review of this manuscript and approving it for publication was Rocco Giofrè.

Some infrastructures already existed in this new move, such as the iridium with its 66 active satellites constellation in providing voice and low data service for cellular phones [5]. In recent years, some space missions have been launched as well such as the Global Express to provide more advanced communications services with high throughput satellites (HTS) [6]. The GEO system has been the most popular approach in terms of providing commercial satellite communication services, however, the propagation delay, attenuation, and higher launching cost makes LEO systems a better choice. The Telesat and Onweb constellation prove further the candidacy of LEO, besides its short propagation, global coverage and low launch cost [1].

Recently, some initiatives have been taken to enhance the 5G network to integrate it with non-terrestrial access technology [25] such as the Third Generation Partnership Project (3 GPP) - R16 plan [7]. It has been believed that this

integration will play an important role in physical attacks and natural disasters, where it will assure reliability, flexibility, and large an efficient broadcast [8]. Furthermore, the space-aerial-terrestrial integrated networks (SATIN), will support the internet of things initiative, where the existing terrestrial 5G networks need to handle a massive amount of data generated by IoT devices and provide connectivity to billions of devices with varying degree of Quality of service (QoS) [9]. However, it is believed that radiation will present a threat in the long term to the mission's performance. This research will address that issue by investigating the first part of the SATIN which is the space network operating in the sub-6-GHz 5G.

The space radiation environment is both complex and dynamic. The earth is surrounded by the Van Allen belt, which is charged with different particles, such as electrons and protons trapped in the Earth's magnetic field. These heavy ions can be hazardous to electronic systems. In recent years, there have been efforts to develop high-frequency space communication technologies using either gallium arsenide (GaAs) or silicon-based devices.

As an electronic device used to filter out the noise and strengthen the input signals received at the front ends of communication systems, the (LNA) is one of the most important components in the satellite [11]. Inside the Among the semiconductor-based devices, silicon germanium (SiGe) and GaAs devices are potentially ideal candidates for the development of wireless communication systems such as low noise amplifiers (LNA) [10].

(LNA), the transistor represents the most important part of its design [12]. Some of the commercial off-the-shelf (COTS) SiGe and GaAs LNAs are used in some receiver modules of the communication systems such as in CubeSats [13].

Previous research works have been investigated different electronics components deployed in space in general and the LNA in particular, and show that major components of satellite communication systems are affected by the characteristics of the radiation environment, [10], [14]–[23].

Therefore, it is of considerable importance to conduct such an investigation on the effect of radiation on both GaAs and SiGe based transistors implemented in LNAs used in LEO space missions. The contribution of this paper lies in elucidating the radiation impacts on components and devices deployed in space missions, and subsequently deteriorating the performance at the system level in the long term. Specifically, the Gallium-Arsenide (GaAs) pseudomorphic high electron mobility transistor (pHEMT) based and the Silicon-Germanium (SiGe) Heterojunction Bipolar Transistor (HBT) based LNAs were irradiated using electron radiation and the effect of their performance was quantified in terms noise figure and the S- parameters, under different radiation doses. Furthermore, the performance degradation of the communication link, employing both types of LNAs, under electron radiation were quantified in terms of the achievable signal to noise ratio (SNR) and the bit error rate (BER).

This paper is organized as follows: Section II presents the SATIN architecture, Section III presents the irradiation process and measurement of the LNAs, Section IV the experiment results from the discussion, and highlighting the orbit performance degradation of the communication system, and Section V the conclusion.

II. THE SPACE-AERIAL-TERRESTRIAL INTEGRATION NETWORKS

A. THE SATIN ARCHITECTURE

Studies have been shown that the integration between the space, aerial and terrestrial networks have been reported to be an excellent choice to reinforce the 5G network, in case of natural disaster and physical attack. The same studies demonstrate the advantages of the SATIN in terms of global coverage where it will promote the 5G network in isolated areas such as Islands and mountains. Most importantly the SATIN will increase the reliability of the 5G, in strengthening the smooth continuity of the internet of things devices and other platforms. Moreover, the SATIN could provide a large footprint that will help improve the scalability of 5G in broadcasting.

As reported in figure 1, the SATIN will be composed of Radio Access Networks (RAN) and Core Networks (CN). Starting with the space access network that encapsulates the GEO, MEO, and LEO satellite constellations. The aerial access network will assume the communication of aerial vehicles, while the terrestrial access network will ensure the smooth terrestrial communication systems through the 3GPP and the non- 3GPP access. Finally, the core network will handle many access networks in terms of data management, policy controls, and others [24], [25].

5G is envisioned to provide ubiquitous access for various IoT applications. Both the telecommunication industry and satellite industry are aligned on the necessity of satellite integrated 5G. Recently, the 3GPP has initiated the study on the enhanced 5G radio access network (RAN) to accommodate non- terrestrial access technologies. Figure 2 shows the potential 5G RAN architectures oriented to the satellite access. The whole satellite with regenerative payload (gNB) functionalities are realized by the onboard payload of the satellite. The service link is based on the NR-Uu protocol stack, whereas the feeder link can be realized by leveraging existing satellite radio interface technologies. The regenerative payload is responsible for interworking between different radio interfaces. The onboard gNB can establish many connections (Xn) with neighbor gNBs by using ISLs and establish N2/N3 connections with the 5G core network. Since both 5G RAN control plane and the user plane are terminated at the onboard gNB, only the propagation delay of the service link impacts the RAN performance [1].

Given that the integrated 5G system is expected to serve large numbers of users simultaneously, the multiple access mechanism is critical to ensure high system performance and good user experience. Related studies are going now on the implementation of the massive MIMO transmission for LEO satellite communications in exploiting the statistical channel state information (sCSI) with full frequency

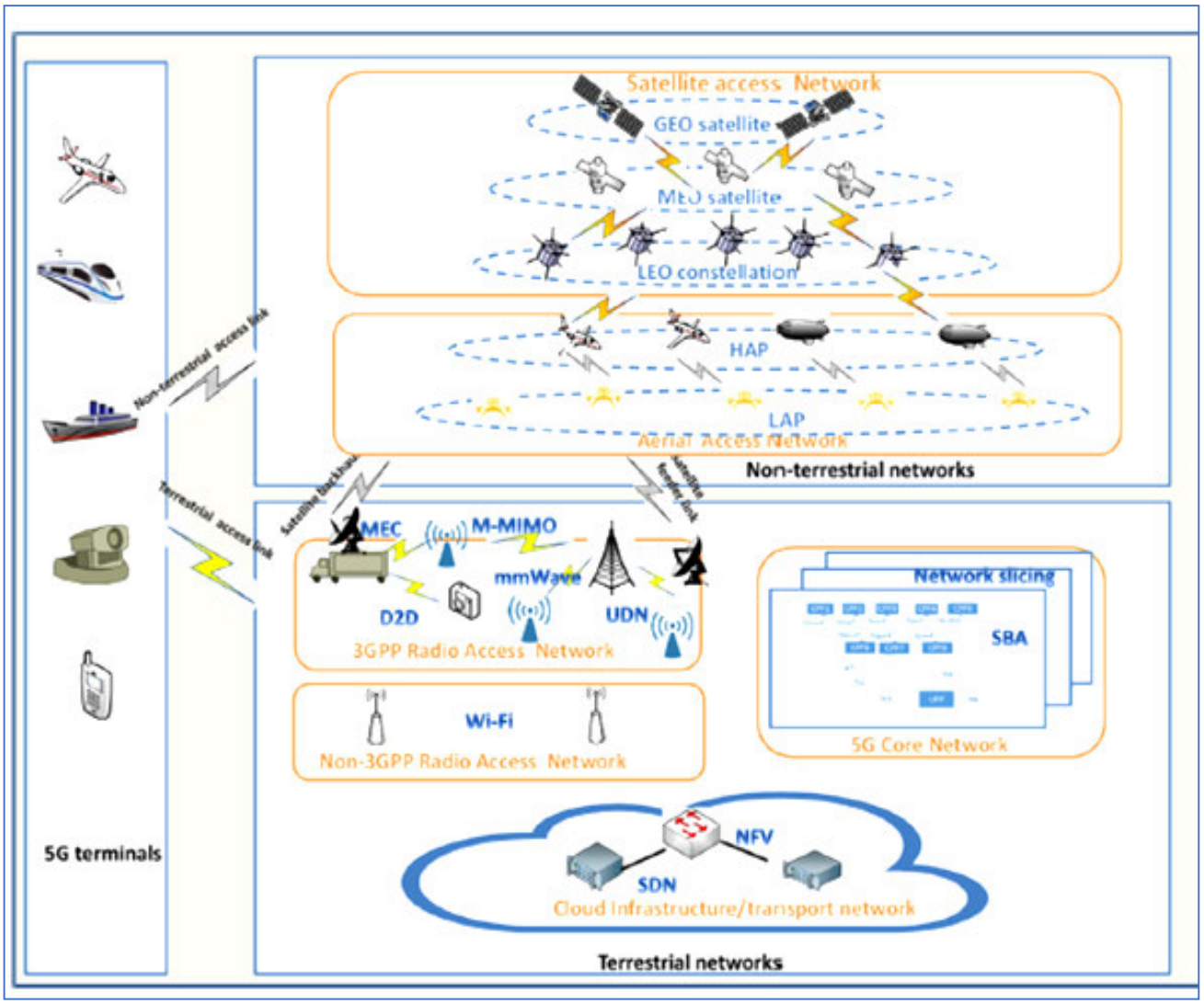

FIGURE 1. Space-aerial-terrestrial integrated 5G architecture [1]. It composed by the space access network, the aerial access network and the terrestrial access network.

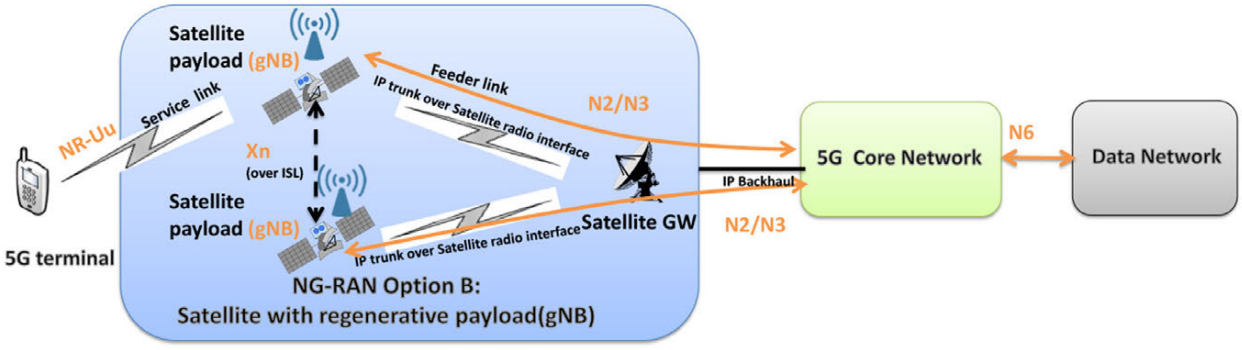

FIGURE 2. Proposed option of a satellite oriented 5G integrated network architecture [1].

reuse. A massive MIMO channel model for LEO satellite communications has been established by taking into account the LEO satellite signal propagation properties and simplified the uplink/downlink transmission designs via performing doppler and delay compensations at user terminals [32].

Currently, orthogonal multiple access (OMA) and non-orthogonal multiple access (NOMA) are two typical multiple access techniques. In OMA The frequency-division multiple access (FDMA), time-division multiple access (TDMA) and code-division multiple access (CDMA) can be considered as

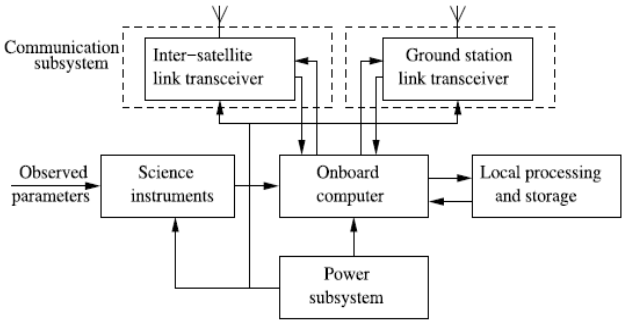

FIGURE 3. Block diagram outlining the main subsystems of a CubeSat. The first part of the communication subsystem connected to the other satellite links and the second part is connected to the ground station [13].

three basic OMA solutions. The OMA has been widely used in terrestrial and satellite communications systems. Recently, the NOMA has received significant attention from academia and industry. NOMA makes it possible for the users in the same cell to use the same channel resources simultaneously. Compared to OMA mechanisms like TDMA and FDMA, NOMA can achieve higher spectrum efficiency. The NOMA is very helpful for the 5G system to fulfill challenging requirements such as extremely high spectrum efficiency and massive connectivity [1].

B. INTER-SATELLITE LINK DESIGN

As it is reported in [1] and demonstrated in [26] LEO presents a niche orbit in establishing the SATIN. Therefore, this research work will be focusing more on the CubeSats launched at that particular orbit as a reference for our investigation. It is almost two decades since the CubeSats have been formally appearing in the space fora. In 2013, hundreds of CubeSats missions have been documented [15]. CubeSats missions can be a single satellite that only communicates to the ground or in constellations where there will be an inter-satellite link and to the ground. The latter will be our main link of interest in our investigation, assuming an inter-satellite radio frequency link operating in the 6-sub-G frequency which can be used by 5G networks, and in particular from 2.3 – 2.7 GHz. For simplicity, the radiation effect will be studied in the range of conventional microwave (at 2.4 GHz, 5 GHz) link.

Nevertheless, these results could be scaled to mm Wave (at 60GHz), and THz (at 300 GHz) communications links integrated with the SATIN 5G. The satellite oriented 5G network architecture is further discussed in the appendix.

The BER will be the parameter to evaluate the link performance in parallel with the signal to noise ratio (SNR) given by:

$$SNR = \frac{E_b}{N_0} = \frac{P^r/R}{kT_s} \tag{1}$$

where the E_b is the energy per bit, N_0 noise spectral density, P_r the received power, R is the data rate, k is the Boltzmann's constant, and T_s is the summation of the antenna noise temperature and receiver noise temperature.

TABLE 1. Example of power budget for cubesat-to-cubesat radio link.

Parameters	Values
Frequency band	S-band
Frequency	2.450 GHz
Link distance	1000 km
Transmit power P_t	15 dBm
Transmitter loss	0.2 dB
Transmit Gain G_t	14.6 /21 dBi
Propagation path loss L_p	100 dB
Other propagation losses	2 dB
Receive gain G_r	14.6 /21 dBi
Receiver noise temperature T_r	1228 K
Antenna noise temperature T_{ant}	22K
System noise T_s	1250 K
Data rate R	1 Mbps
Link Margin	1dB

The received power from the receiver is given in the following equation:

$$P^r = \frac{P_t G_t G_r}{L_p} \tag{2}$$

where P_t and P_r are the transmitted and received power expressed in Watts [W], Gt and Gr are the transmit and receive of the LNA gains in the antenna respectively, and Lp is the propagation path loss given by:

$$L_p = \frac{4\pi df}{c} \tag{3}$$

with d being the distance between the radio transmitter and receiver, f the radio signal frequency, and c the speed of light.

By combining (1), (2), and (3) the SNR can be written:

$$SNR = \frac{E_b}{N_0} = \frac{P_t G_t Gr}{kT_s R L_p} \tag{4}$$

Equation (4) can be written in the following form with decibel:

$$\begin{aligned} SNR_{dB} &= 10\log_{10}\left(\frac{P_t G_t Gr}{kT_s R L_p}\right) \\ &= P_t - 30 + G_t + G_r - L_p - 10\log_{10} k \\ &\quad - 10\log_{10} k - 10\log_{10} T_s - 10\log_{10} R \end{aligned} \tag{5}$$

If we consider BER for BPSK modulation over Gaussian channel, the bit error probability by using the Q- function is given:

$$P_b = Q\left(\sqrt{2\frac{E_b}{N_o}}\right) \tag{6}$$

III. IRRADIATION PROCESS AND MEASUREMENT

A. THE IRRADIATED SAMPLES

The irradiated samples are Analog Device Inc. ADL5523 GaAs and the NXP BFU730F SiGe low noise

amplifiers (LNAs) with a frequency range of 2.3- 2.7 GHz and 400 MHz to 4 GHz respectively.

Figure 4 shows the Gallium-Arsenide (GaAs) pseudo-morphic high electron mobility transistor (pHEMT) is a high-performance GaAs low noise amplifier (LNA) The ADL5523 is a high-performance GaAs low noise amplifier. It provides high gain and low noise figure for single-down conversion IF sampling receiver architectures as well as direct-down conversion receivers. The ADL5523 provides a high level of integration by incorporating the active bias and the dc blocking capacitors, making it very easy to use while not sacrificing design flexibility. The device can support operation from 3V to 5V, but we operate at 3V similar to the SiGe supply voltage. The current draw can be adjusted with the external bias resistor for applications requiring very low power consumption [27].

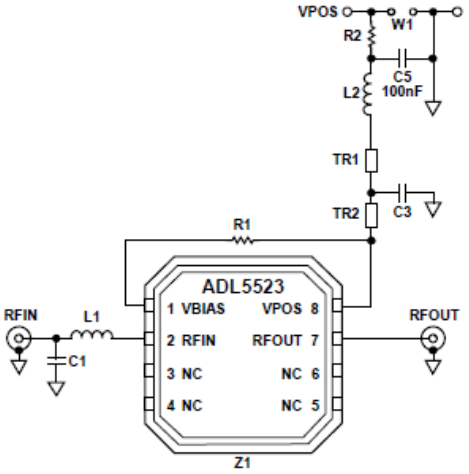

FIGURE 4. Schematic diagram of ADL5523 GaAs LNA. Capacitor C5 provides the power supply decoupling. Inductor L1 and capacitor C1 provide the input impedance matching and L2 and C3 for output impedance matching. Resistor R1 is used to set the supply current.

While in figure 5 represents the BFU730F 2.3-2.7GHz LNA is a discrete HBT manufactured by NXP Semiconductors. advanced shows the circuit of the BFU730F. The BFU730F is a discrete HBT that is produced using NXP Semiconductors' advanced 110 GHz fT SiGe: C BiCmos process. SiGe: C is a normal silicon germanium process with the addition of Carbon in the base layer of the NPN transistor. The presence of carbon in the base layer suppresses the boron diffusion during wafer processing. This allows steeper and narrower SiGe HBT base and a heavier doped base. As a result, lower base resistance, lower noise and higher cut off frequency can be achieved.

It can be highlighted that these two technologies have comparable frequency response, and to better compare them, we chose devices with the same emitter area approximately.

Neither technology has been intentionally optimized for radiation tolerance. The investigation is based generally on the noise figure and S-parameters.

It has been found in previous related investigations that the radiation could cause an increase in the base current at low

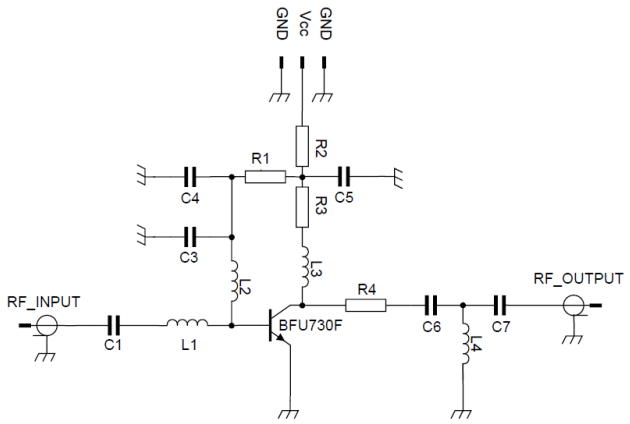

FIGURE 5. Schematic of the BFU730F SiGe LNA. The LNA consist of one stage grounded emitter BFU730F amplifier. The LNA shows a gain of 20 dB, NF of 0.8 dB.

bias in both the technologies. In the low bias region, the base current is usually dominated by the generation-recombination current. These radiation-induced generation-recombination centers will decrease the current gain in the low bias regime for both technologies. It has been found as well the degradation of the noise figure (NF) in both technologies due to the degradation of the current gain, cutoff frequency, and the base-emitter resistance in the RF bias region [17].

The choice of this frequency range is to consider the sub-6 GHz range (FR1) of 5G and given the fact that some CubeSats missions at LEO are operating in the L- S-band [13]. Moreover, some other information of the link design infer the RazakSAT-1 launched in 2009, as part of the Malaysian Satellite program, as reported in [28]

B. IRRADIATION PROCESS AND MEASUREMENT EXPERIMENTAL SETUP

The space radiation environment especially at Low Earth Orbit is populated with a trapped particle at Van Allen Belts, galactic cosmic ray, and other radiation from the sun. Among those particles are protons and electrons radiation, which may cause total ionizing dose (TID), displacement damage (DD), single event effect (SEE) and others, imposing the space mission in LEO at risk [35]. The electron radiation at LEO is estimated to be ranged from 100 Kev – 1 Mev [28].

Thanks to the EPS – 3000 electron beam machine facility in Nuclear Malaysia, could provide up to 3 MeV of electron radiation. For considering the worst-case scenario and with reference to Suparta [31], The LNAs samples were irradiated with 1.5 MeV electrons of energy with five iterations of radiation exposure of electron-equivalent doses ranging from 50 kGy to 250 kGy, at the Malaysian Nuclear Agency.

All measurements were carried out in the RF Laboratory, faculty of engineering IIUM. To produce and assure accurate measurement results, the Agilent N5230A vector network analyzer (VNA) went through a series of calibration procedures to cancel the effect of cable losses or any other losses associated with both input and output ports. Furthermore,

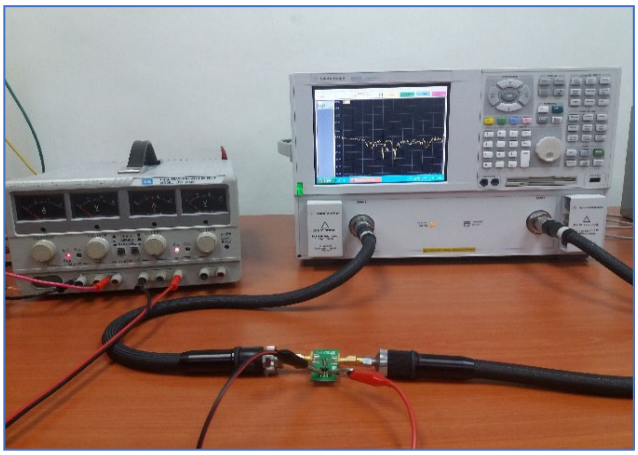

FIGURE 6. S- Parameters measurement experimental setup using the Agilent N5230A Vector Network Analyzer (VNA). A voltage of 3V is fed into the LNAs by a power supply.

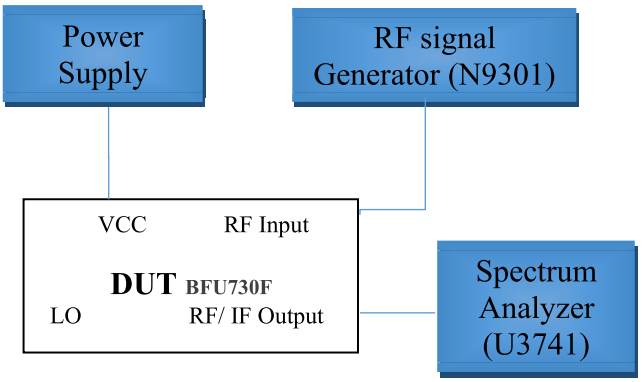

FIGURE 7. Gain method to measure Noise figure measurement experimental set up. It involves measurements as well as calculations.

all our RF Lab equipment is audited for calibration by the suppliers in a systematic yearly exercise. Figure 6 shows the experimental set-up for the measurement process of the scattering parameters using the (VNA) with a power supply. The noise figure can be measured with different methods such as the reported in [34]. For our investigation, the measurement of the noise figure is determined with the Gain method [30], using the Spectrum Analyzer, model U3731with RF signal generator N9301, as reported in figure 7.

IV. RESULTS AND DISCUSSION

A. THE NOISE FIGURE (NF)

The noise figure vs. frequency for the GaAs pHEMT and the SiGe HBTs, are reported in Figures 8 and 9 respectively. It shows the result of the noise figure for pre-and post-irradiation up to 250 kGy electron total doses taken at 3V. It can be observed in Figure 8 that the noise figure of GaAs was 0.9 dB at 2.3 GHz before irradiation. After the first exposure of 50 kGy, there were no significant changes seen at the low frequency. However, as the frequency increases, a little degradation around 1dB was observed at 2.7 GHz.

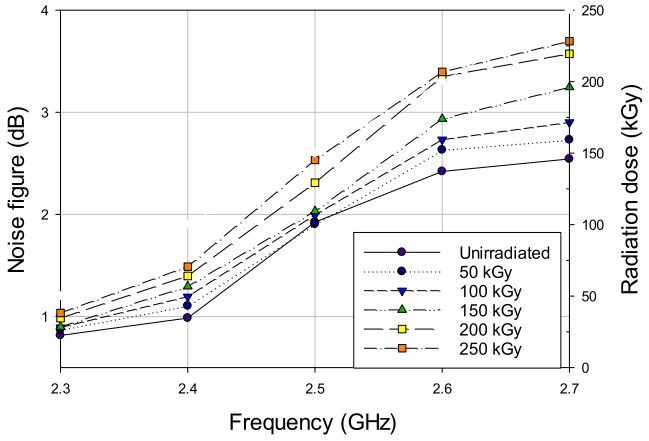

FIGURE 8. GaAs (LNA) noise figure as a function of the frequency and radiation dose at (3V). The radiation dose is ranged from 50 kGy to 250 kGy. The noise increases with the increase in the frequency and radiation dose.

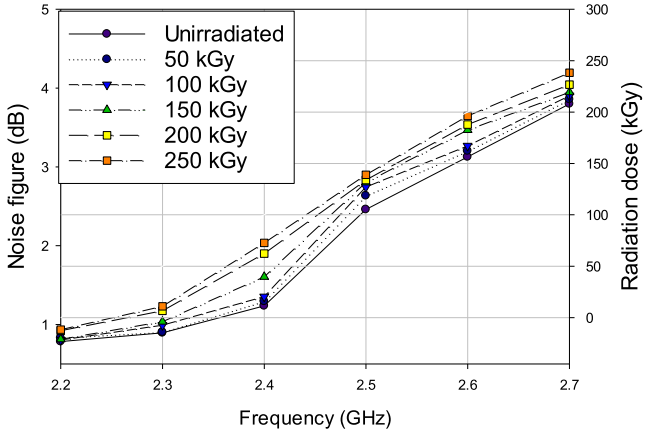

FIGURE 9. SiGe (LNA) noise figure as a function of the frequency and radiation dose at (3V). The noise increases with the increase of the frequency and radiation dose.

In Figure 9, the noise figure increases by 0.8 dB with the first radiation dose, along with the frequency range from 2.3 GHz to 2.7 GHz. The noise figure keeps increasing gradually with the increase of the radiation dose. After the final dose of 250 kGy, the noise figure degraded further as its doubles.

To further illustrate the comparison between both (NF), Figure 10 represents both (NF) of the GaAs and SiGe LNAs versus frequency. It can be observed that both LNA noise figures are approximately consistent in the frequency range before radiation.

However, after radiation, the GaAs LNA noise figure is approximately 2.8 dB at 2.3 GHz, and 3.2 dB at 2.7 GHz, while the SiGe LNA is independent of the increment of the frequency compared to GaAs. It can be highlighted that the change in frequency affects the performance of the GaAs LNA in terms of noise figure more than the SiGe LNA.

Figure 11 represents the noise figure for both LNAs versus radiation doses. It can be observed that with the increment of doses, in general, both noise figures of the LNAs are increasing. However, it can be identified that the frequency is

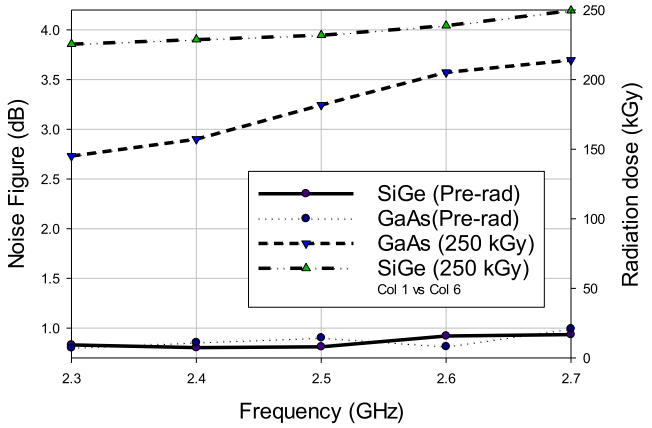

FIGURE 10. The noise figure as a function of the frequency of SiGe and GaAs (LNA) at (3 V) for the pre-irradiation and 250 kGy radiation dose. The SiGe LNA noise figure is more than 4 dB, while the GaAs increase with the radiation dose up to 3.7 dB, with an exhibition of frequency sensitivity compared to the SiGe LNA.

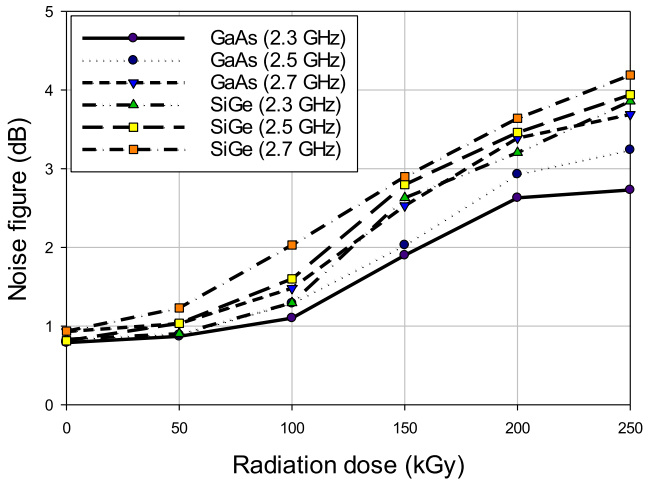

FIGURE 11. The noise figure as a function of the radiation doses of SiGe and GaAs (LNA) at (3 V) for pre-irradiation and the reported different radiation doses. The effect of the high frequency on the LNA performance can be seen.

making a difference in the GaAs LNA compare to the SiGe as mentioned earlier. In other words, by increasing the frequency at a particular radiation dose, the noise figure is noticeably increasing differently, while the SiGe, the degradation of the noise figure is consistent with increasing the radiation dose for different frequencies.

For 100 kGy and below, the noise figure increased by 0.2 dB approximately. While for more than 100 kGy, the noise figure increased by more than 1 dB. The degradation of the noise figure for both the SiGe and the GaAs HBT is due to the small degradation of beta, the cut off frequency, and the base-emitter resistance in the RF bias region [16]. The radiation could cause an increase in the base current at low bias in SiGe and GaAs technologies. In the low bias region, the base current is usually dominated by the generation-recombination current. These radiation-induced generation-recombination centers will decrease the current gain in the low bias region for SiGe and GaAs as well the noise figure (NF) due to the

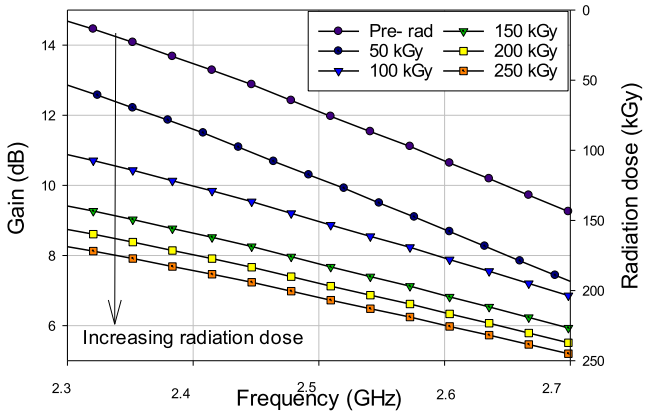

FIGURE 12. GaAs (LNA) Gain (S21) as a function of the frequency and radiation dose at (3V). The Gain decreases with the increase of the frequency and radiation dose. The radiation effect is more significant at 50 kGy to 100 kGy, compared from 150 kGy to 250 kGy.

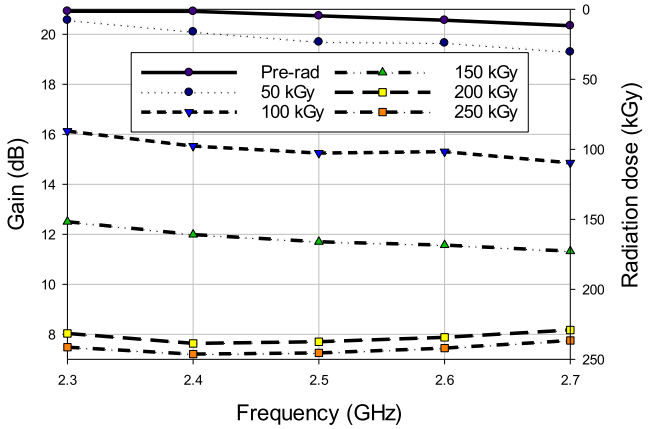

FIGURE 13. SiGe (LNA) Gain (S21) as a function of the frequency and radiation dose at (3V). The Gain decreases with the increase of the radiation dose. The effect of the increase of the frequency has less impact on the gain.

degradation of the current gain, cutoff frequency, and the base-emitter resistance in the RF bias region [17].

Overall, up to 250 kGy, the GaAs and SiGe LNA noise figures show electron radiation hardness. Although there is a degradation in both the LNA noise figures, they exhibit a tolerance of the increase of the radiation doses where the degradation is less than 1dB for every 50 kGy up to 250 kGy.

B. THE GAIN (S21)

The pre and post gain of the irradiated results of both LNAs are reported in figure 12 and figure 13. Figure 12 shows the gain of the GaAs LNAs with a maximum value of 14.67 dB at 2.1 GHz before irradiation. The datasheet reports a gain of 15dB at 2.6 GHz, while our measurement at 2.3 GHz reads 14.67dB. For the first radiation exposure of 50 kGy of radiation, the gain consistently decreased by approximately 1.5 dB within the frequency range.

After the third exposure of 150 kGy of electron radiation, the gain decreases by less than 1 dB throughout the frequency range. Overall, the gain has been decreased by 6.5 dB

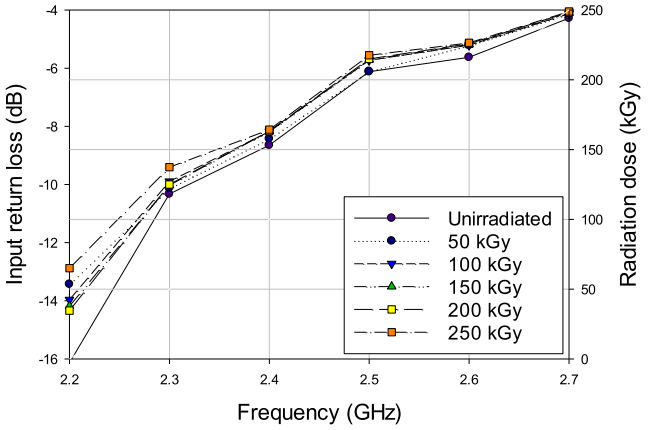

FIGURE 14. GaAs (LNA) input return loss (S11) as a function of the frequency and radiation dose at (3V). The input return loss is increasing with the radiation dose and the increase is noticed at low frequency.

approximately. The degradation of the GaAs gain is because of the decrease in the effective minority-carrier lifetime (τ) of the n-type emitter and due to the decrease in the electron mobility (μ n) which will cause the gain to drop [16].

In figure 13 shows the SiGe LNA's gain. It shows a linear response within the frequency range of 2.3 GHz to 2.7 GHz. The gain decreases rapidly with the increment of the radiation dose. For instance, it can be observed that the gain was on average of 20 dB within the frequency range before irradiation. After 50 kGy electrons. Magnetization 100 and 150 kGy, the gain degraded severely to 15 dB and 10dB, respectively [23].

The overall gain degradation for the SiGe HBT has been due to the total ionization dose (TID) and displacement damage (DD). The TID creates oxide trapped charges and interface spaces in the emitter-base spacer that minimally increases base current leakage in SiGe HBTs, which consequently degrades the gain. For the (DD), it shortens the hole (minority carrier) lifetime, which is inversely proportional to the base current, thus degrading the base current and gain in turn for both gains within the entire range of the bandwidth of interest [23].

C. THE INPUT RETURN LOSS (S11)

The (S11) is the input port voltage reflection coefficient at port 1 when port 2 is matched. The GaAs post-irradiation of the input return loss (S11) is shown in figure 14. It shows that the degradation took place in lower frequencies up to 2.5 GHz, while from 2.5 GHz upwards, there is no significant difference between pre-and post-irradiation for the S11, as it keeps steady with a marginal increase that is approximated to 1 dB as the radiation dose increases.

Figure 15 shows the input return loss (S11) of the SiGe LNA versus frequency. It can be seen that at 50 kGy there is a major shift of up to 8 dB, particularly higher frequencies. By increasing the dose from 100 kGy up to 250 kGy, a moderate increase of the return loss is observed. However, as the frequency is increasing beyond 2.4 GHz, there is a substantial

TABLE 2. Comparison of the degradation of the LNA gain.

Ref.	Radiation type	Freq. (GHz)	Gain (dB) after irradiation		NF (dB) After irradiation		Technology
			Pre-	post	Pre-	post	
[15]	Proton	8 -18	32.5	28	8	11.5	SiGe
[16]	Gamma	0.5-10	-	-	2.3	2.6	GaAs
			-	-	3	3.1	SiGe
[17]	Proton	8- 16	17.5	16	5.74	9.7	SiGe
This work	Electron	2.3 – 2.7	14.6	8.24	1	2.15	GaAs
			21	8	0.8	3.9	SiGe

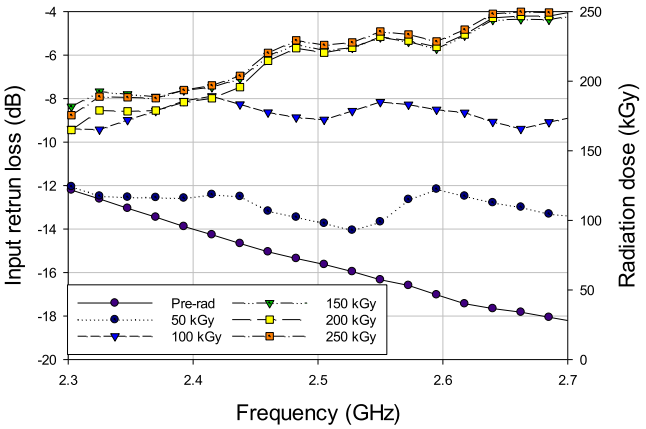

FIGURE 15. SiGe (LNA) input return loss (S11) as a function of the frequency and radiation dose at (3V). The SiGe input return loss is increasing with the radiation dose especially at a higher frequency.

degradation in the return loss as the radiation is incremented, reaching up to 4dB. This is in parallel with [16], it has been reported that the increase of the input return loss is due to single event effects (SEE) directly from electrons. When energy is deposited by the incident, photons, or high velocity charged particles, it produces traps or induces incomplete bonding at surfaces, both of which will generally lead to excess leakage, shifts in operating points, and performance degradation.

D. THE OUTPUT RETURN LOSS (S22)

The output return loss (S22) of the GaAs LNA is shown in figure 16. We can observe that the output loss decreases with the increase in the radiation dose. Comparing the worst case, which has a higher frequency with −5dB approx. of output return loss, the output return loss here is approximately −7 dB after radiation. We can see an improvement in S22 performance. At lower frequencies below 2.4 GHz, there is a slight improvement compared to the higher frequencies ranging from 2.4 GHz up to 2.7 GHz with an improvement f ∼ −1dB, as before radiation, the mean value was −6 dB,

TABLE 3. Theoretical calculations of the performance degradation of the communication under electron radiation.

	Parameter	Radiation dose					
		Unirradiated	50 kGy	100 kGy	150 kGy	200 kGy	250 kGy
SiGe LNA	SNR (dB)	31	29	21	15	7	5
	BER	1.7×10^{-8}	1.3×10^{-14}	4.6×10^{-11}	2.2×10^{-8}	9.7×10^{-5}	8.5×10^{-4}
GaAs LNA	SNR (dB)	20	17	12.54	9.62	8.22	7.3
	BER	1.3×10^{-10}	2.8×10^{-9}	2.8×10^{-7}	6×10^{-6}	2.6×10^{-5}	7×10^{-3}

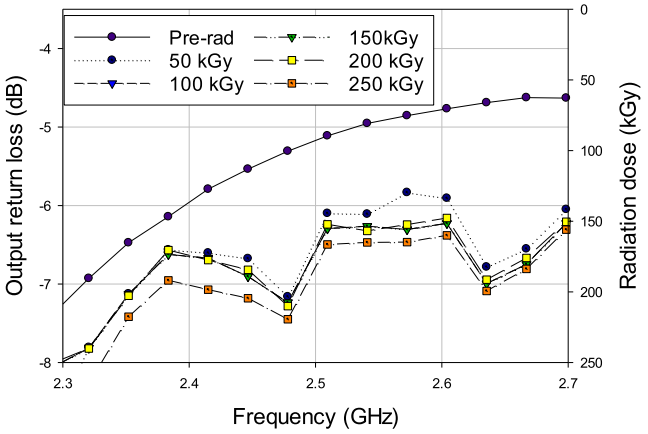

FIGURE 16. GaAs Output Return Loss (S22) as a function of the frequency and radiation dose at (3V). The GaAs output return loss is decreasing with the radiation dose.

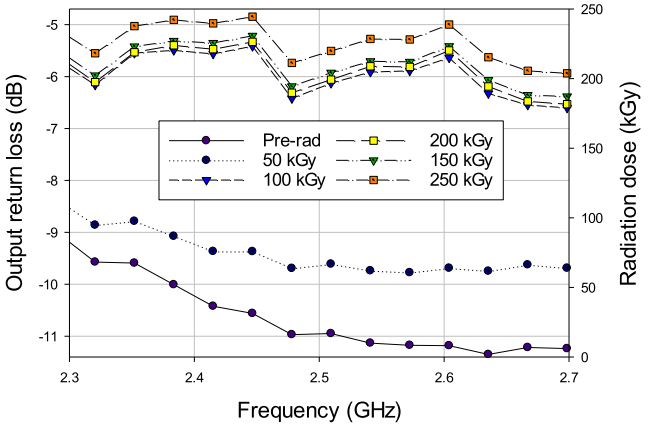

FIGURE 17. SiGe Output Return Loss (S22) as a function of the frequency and radiation dose at (3V). The SiGe output return loss is increasing with the radiation dose.

and then after radiation, the S22 reduced to −7 dB as a mean value as shown in the figure.

According to [23], the improvement could be due to the radiation-induced improvement of electronic properties (e.g., mobility, the minority carrier lifetime) at low dose irradiation, as reported in GaAs devices in previous works.

It has been reported also that irradiation may restructure the semiconductor crystal, thus leading to the improvement of the electronic properties. While such an improvement in the

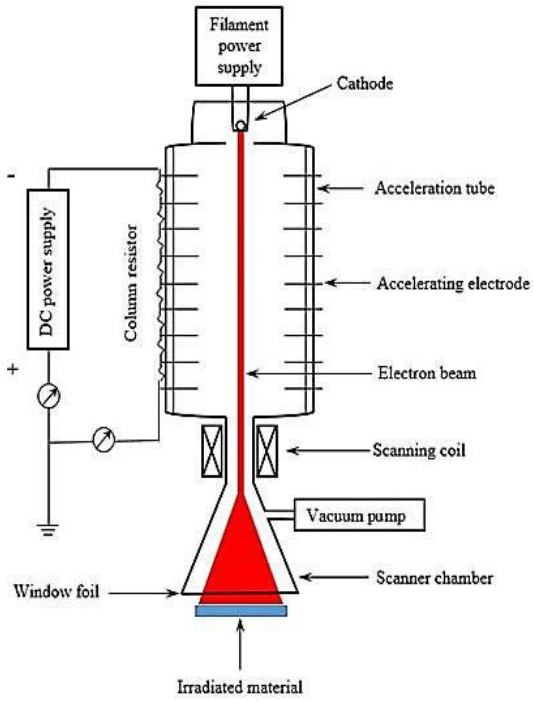

FIGURE 18. Structural arrangement of EPS-3000 electron beam machine (Kashiwagi, 2012).

crystal structure may be, in principle, possible, the arguments presented above offer an alternative plausible explanation for the output return loss improvement in our LNA. However, the output return loss of the SiGe LNA is affected by the radiation, as reported in Figure 17. Gradual degradation after each dose is observed, where the initial mean value was below -9 dB to a mean value of -5 dB after 250 kGy dose exposure. This can be explained by the fact that, in SEE, while both drift and diffusion charge collection from the collector – substrate are effectively eliminated, the collector-base junction drift charge will continue to play a significant role [19].

Table 2 shows the GaAs and SiGe LNAs' gains and NF compared to other wideband LNAs operating in a similar frequency range. It shows that both LNAs can still work after 250 kGy electron exposure when compared with other state-of-the-art LNAs.

However, it can be deduced that both LNAs will die out when radiation doses increase, given that the S21 for both

LNA rolls off systematically with the increase of electron radiation.

E. ON ORBIT PERFORMANCE OF THE INTER-SATELLITE LINK UNDER ELECTRON RADIATION

To further investigate, a radio link was analytically designed as reported in Table 1, and the gain of both LNAs have been implemented in the system, using equations (5) and (6). The performance of the link under the influence of the electron irradiation can be calculated in terms of the bit error rate (BER) and signal to noise ratio (SNR), considering the BPSK modulation technique.

Table 3 reported the link performance implementing the GaAs and SiGe based LNAs under the effect of electron irradiation. The degradation of the gain is fed into equation (5) to calculate the SNR, and then deduce the BER from equation (6). It was observed that the system will work properly up to 150 kGy, as the BER is still in the accepted range [26]. However, after 150 kGy of electron irradiation, the system will be degraded. This is in turn will influence as well the performance of the space-aerial-terrestrial 5G network links. In this investigation, the transceiver gain was the parameter put into evidence while assuming other parameters constant.

V. CONCLUSION

This paper investigates the electron radiation effect on GaAs and SiGe low noise amplifiers-based technologies. Generally, both LNAs have been degraded because of electron radiation.

At the circuit level, the noise figure of GaAs LNA is less degraded by electron radiation as compared to the SiGe LNA by more than 0.5 dB at the highest radiation dose. The gain of SiGe LNA was less dependent on the frequency increase.

However, it was decreasing rapidly with the radiation dose increment. The GaAs LNA, is sensitive to the frequency increase, but demonstrate some robustness under radiation as it decreased by 20 % compared to the SiGe.

The input and output return losses (S11) and (S22) for both SiGe and GaAs increased with radiation, except the output return loss (S22) of the GaAs, which shows improvement after electron radiation. This could be due to stability and the improvement of the crystal lattice arrangement. Overall, the ADL5523 GaAs LNA performed well compared to the NXP BFU730F SiGe LNA under electron radiation up to 250 kGy.

At the system level, the performance of the RF inter-satellite communication link will be influenced when the radiation dose reaches 150 kGy where the BER is $6\times10^{-6}6 \times 10^{-6}$, which is less than the accepted range of the satellite communication system. This performance degradation shows that a higher level of radiation may jeopardize the SATIN G5 networks.

This investigation focused on the gain of the transceiver, but we believe that other electronic components should be further studied such a particular situation of a harsh space radiation environment. This is to ensure that adequate radiation hardness measures will be put into consideration accordingly, to assure the effectiveness and reliability of the SATIN 5G network projects.

TABLE 4. Main parameters of EPS-3000 electron beam machine.

Energy (MeV)	Beam current (mA)	Maximum beam power, (kW)	Beam width/area. cm	Conveyor speed, m/min
0.5-3.0	1-30	90	30, 60 and 120	1-20

APPENDIX

THE EPS–3000 ELECTRON BEAM MACHINE

Electron irradiation was performed at the Malaysian Nuclear Agency (MNA) using an EPS-3000 electron beam machine. The EPS-3000 electron beam machine (EPS-3000 EBM) is the first of its kind in Malaysia and was installed in MNA in 1991. The machine was manufactured by Nissin High Voltage and is currently used for commercial irradiation and R&D in surface curing and modification (Siti Aiasah Hashim, 2012).

ACKNOWLEDGMENT

The authors would like to thank Nuclear Malaysia Agency for allowing us access to the Alurtron facility to conduct the irradiation process. They also would like to specially thank the engineers in the Alurtron facility for their assistance and cooperation during the electron irradiation process.

The main parameters of EPS-3000 are given in Table 4. The operation principle of the electron beam machine can be explained as follow; heated tungsten film (cathode) generates electrons that are drawn and accelerated by accelerating electrodes through the acceleration tube (Figure 18). As the electron beam passes from the acceleration tube and through the scanning coil, an oscillating magnetic field sweeps the beam back and forth across the scanner chamber. Then electrons proceed through the window foil from vacuum to the normal atmosphere and penetrate the material. The doses of this experiment are ranged from 50 kGy to 200 kGy, using on average 2- Mev at room temperature based on previous related investigations (H.Johnston, 2003).

REFERENCES

[1] S. Zhang, D. Zhu, and Y. Wang, "A survey on space-aerial-terrestrial integrated 5G networks," *Comput. Netw.*, vol. 174, Jun. 2020, Art. no. 107212.
[2] W. G. NetWorld2020's–SatCom, "The role of satellites in 5G, version 5," NetWorld Eur., Secretariat Eurescom: Eurescom GmbH, Heidelberg, Germany, White Paper, Jul. 2014, pp. 1–20.
[3] M. Jia, X. Zhang, X. Gu, X. Liu, and Q. Guo, "Joint UE location energy-efficient resource management in integrated satellite and terrestrial networks," *J. Commun. Inf. Netw.*, vol. 3, no. 1, pp. 61–66, Mar. 2018.
[4] B. G. Evans, "The role of satellites in 5G," in *Proc. 7th Adv. Satell. Multimedia Syst. Conf.*, 2014, pp. 197–202.
[5] Y. Su, Y. Liu, Y. Zhou, J. Yuan, H. Cao, and J. Shi, "Broadband LEO satellite communications: Architectures and key technologies," *IEEE Wireless Commun.*, vol. 26, no. 2, pp. 55–61, Apr. 2019.
[6] H. L. B. Zhou, "Development review of foreign emerging commercial LEO satellite communication constellations," *Telecommun. Eng.*, vol. 58, no. 9, pp. 1108–1114, 2018.
[7] *Solutions for NR to Support Non-Terrestrial Networks*, document TR 38.821, 3GPP, 2016, vol. 16.

[8] *Study on Using Satellite Access in 5G*, document TR 38.811, 3GPP, 2015, vol. 15.

[9] M. Tahir, M. H. Habaebi, M. Dabbagh, A. Mughees, A. Ahad, and K. I. Ahmed, "A review on application of blockchain in 5G and beyond networks: Taxonomy, field-trials, challenges and opportunities," *IEEE Access*, vol. 8, pp. 115876–115904, 2020.

[10] J. D. Cressler, "Radiation effects in SiGe technology," *IEEE Trans. Nucl. Sci.*, vol. 60, no. 3, pp. 1992–2014, Jun. 2013.

[11] M. A. Bashir, M. M. Ahmed, U. Rafique, and Q. D. Memon, "Design of a Ku-band high gain low noise amplifier," in *Proc. IEEE Int. RF Microw. Conf. (RFM)*, Penang, Malaysia, Dec. 2013, pp. 168–171.

[12] T. Noji, A. Miyachi, T. Kikuchi, N. Y. Yamasaki, K. Mitsuda, and S. Kawasaki, "The X-band high gain and radiation-hardness low-noise GaAs MMIC amplifier with cryogenic temperature for X-ray astronomy," in *Proc. Asia–Pacific Microw. Conf.*, Sendai, Japan, 2014, pp. 160–162.

[13] O. Popescu, "Power budgets for cubesat radios to support ground communications and inter-satellite links," *IEEE Access*, vol. 5, pp. 12618–12625, 2017.

[14] B. Mossawir, I. R. Linscott, U. S. Inan, J. L. Roeder, J. V. Osborn, S. C. Witczak, E. E. King, and S. D. Lalumondiere, "A TID and SEE radiation-hardened, wideband, low-noise amplifier," *IEEE Trans. Nucl. Sci.*, vol. 53, no. 6, pp. 3439–3448, Dec. 2006.

[15] D. C. Howard, A. S. Cardoso, Z. E. Fleetwood, N. E. Lourenco, T. D. England, P. K. Saha, S. Shankar, R. M. Diestelhorst, E. X. Zhang, C. X. Zhang, P. Paki-Amouzou, and J. D. Cressler, "Mitigation of total dose performance degradation in an 8–18 GHz SiGe reconfigurable receiver," *IEEE Trans. Nucl. Sci.*, vol. 61, no. 6, pp. 3226–3235, Dec. 2014.

[16] S. Zhang, G. Niu, J. D. Cressler, S. J. Mathew, U. Gogineni, S. D. Clark, P. Zampardi, and R. L. Pierson, "A comparison of the effects of gamma irradiation on SiGe HBT and GaAs HBT technologies," *IEEE Trans. Nucl. Sci.*, vol. 47, no. 6, pp. 2521–2527, 2000.

[17] D. C. Howard, P. K. Saha, S. Shankar, R. M. Diestelhorst, T. D. England, N. E. Lourenco, E. Kenyon, and J. D. Cressler, "An 8–16 GHz SiGe low noise amplifier with performance tuning capability for mitigation of radiation-induced performance loss," *IEEE Trans. Nucl. Sci.*, vol. 59, no. 6, pp. 2837–2846, Dec. 2012.

[18] D. Chen, W. Pan, P. Jiang, J. Jin, T. Mo, and J. Zhou, "Reconfigurable dual-channel multiband RF receiver for GPS/Galileo/BD-2 systems," *IEEE Trans. Microw. Theory Techn.*, vol. 60, no. 11, pp. 3491–3501, Nov. 2012.

[19] J. D. Cressler, "Silicon-germanium as an enabling technology for extreme environment electronics," *IEEE Trans. Device Mater. Rel.*, vol. 10, no. 4, pp. 437–448, Dec. 2010.

[20] C. Florian, R. P. Paganelli, and J. A. Lonac, "12-W *X*-band MMIC HPA and driver amplifiers in InGaP-GaAs HBT technology for space SAR T/R modules," *IEEE Trans. Microw. Theory Techn.*, vol. 60, no. 6, pp. 1805–1816, Jun. 2012.

[21] D. C. Howard, J. Poh, T. S. Mukerjee, and J. D. Cressler, "A 3–20 GHz SiGe HBT ultra-wideband LNA with gain and return loss control for multiband wireless applications," in *Proc. 53rd IEEE Int. Midwest Symp. Circuits Syst.*, Seattle, WA, USA, Aug. 2010, pp. 445–448.

[22] Y. Shi, L. Hong-Liang, Z. Yu-Ming, Z. Yi-Men, Z. Jin-Can, and Z. Hai-Peng, "The effects of gamma irradiation on GaAs HBT," in *Proc. IEEE Int. Conf. Electron Devices Solid-State Circuits*, Tianjin, China, Nov. 2011, pp. 1–2.

[23] J. Metcalfe, D. E. Dorfan, A. A. Grillo, A. Jones, D. Lucia, F. Martinez-McKinney, M. Mendoza, M. Rogers, H. F.-W. Sadrozinski, A. Seiden, E. Spencer, M. Wilder, J. D. Cressler, G. Prakash, and A. Sutton, "Evaluation of the radiation tolerance of SiGe heterojunction bipolar transistors under 24-GeV proton exposure," *IEEE Trans. Nucl. Sci.*, vol. 53, no. 6, pp. 3889–3893, Dec. 2006.

[24] A. Gupta and R. K. Jha, "A survey of 5G network: Architecture and emerging technologies," *IEEE Access*, vol. 3, pp. 1206–1232, 2015.

[25] D. Pareit, B. Lannoo, I. Moerman, and P. Demeester, "The history of WiMAX: A complete survey of the evolution in certification and standardization for IEEE 802.16 and WiMAX," *IEEE Commun. Surveys Tuts.*, vol. 14, no. 4, pp. 1183–1211, 2012.

[26] M. Samsuzzaman, M. T. Islam, S. Kibria, and M. Cho, "BIRDS-1 CubeSat constellation using compact UHF patch antenna," *IEEE Access*, vol. 6, pp. 54282–54294, 2018.

[27] *400 MHz to 4000 MHz Low Noise Amplifier Data Manual*, Analogue Devices, Norwood, MA, USA, 2017.

[28] W. Suparta and S. K. Zulkeple, "Simulation of major space particles toward selected materials in a near-equatorial low Earth orbit," *Astrophys. Space Sci.*, vol. 362, no. 5, May 2017.

[29] M. A. Xapsos, P. M. O'Neill, and T. P. O'Brien, "Near-Earth space radiation models," *IEEE Trans. Nucl. Sci.*, vol. 60, no. 3, pp. 1691–1705, Jun. 2013.

[30] *Noise Figure Measurement Methods and Formulas*, Maxim Integrated, San Jose, CA, USA, 2003.

[31] *Single-Stage 2.3_2.7GHz LNA With BFU730F*, NXP Semiconductors, Eindhoven, The Netherlands, 2016.

[32] W. Suparta and S. K. Zulkeple, "Investigating space radiation environment effects on communication of Razaksat-1," *J. Aerosp. Technol. Manage.*, vol. 10, pp. 1–12, May 2018.

[33] L. You, K.-X. Li, J. Wang, X. Gao, X.-G. Xia, and B. Ottersten, "Massive MIMO transmission for LEO satellite communications," *IEEE J. Sel. Areas Commun.*, vol. 38, no. 8, pp. 1851–1865, Aug. 2020.

[34] A. Caglar and M. B. Yelten, "Design of cryogenic LNAs for high linearity in space applications," *IEEE Trans. Circuits Syst. I, Reg. Papers*, vol. 66, no. 12, pp. 4619–4627, Dec. 2019.

[35] S. Ilik, A. Kabaoglu, N. Sahin Solmaz, and M. B. Yelten, "Modeling of total ionizing dose degradation on 180-nm n-MOSFETs using BSIM3," *IEEE Trans. Electron Devices*, vol. 66, no. 11, pp. 4617–4622, Nov. 2019.

ABDOURAOUF SAID YOUSSOUF received the degree and the master's degree, in 2014 and 2016, respectively. He is currently pursuing the Ph.D. degree with the Department of Electrical and Computer Engineering, International Islamic University Malaysia. His research interests include space radiation and optical communications.

MOHAMED HADI HABAEBI (Senior Member, IEEE) received the degree from the Civil Aviation and Meteorology High Institute, Libya, in 1991, the M.Sc. degree in electrical engineering from Universiti Teknologi Malaysia, in 1994, and the Ph.D. degree in computer and communication system engineering from University Putra Malaysia, in 2001. He is currently a full-time Professor and the Post Graduate Academic Advisor with the Department of Electrical and Computer Engineering, International Islamic University Malaysia, where he also heads the research works on the Internet of Things. He has supervised many M.Sc. and Ph.D. students, published more than 120 articles and papers, and sits on the Editorial Boards of many international journals. He is actively publishing in M2M communication protocols, wireless sensor and actuator networks, cognitive radio, small antenna systems, radio propagation, and wireless communications and network performance evaluation. He is an Active Member of the IEEE and an Active Reviewer of many international journals.

NURUL FADZLIN HASBULLAH received the B.Eng. degree (Hons.) from Cardiff University, Wales, in 2001. Later, she worked as an Integrated Chip Design Engineer with Malaysia Microelectronics Solution, Cyberjaya, for a year before joining academia. In 2003, she joined International Islamic University Malaysia, where she is currently an Associate Professor with the Department of Computer Engineering. Her research interests include semiconductor devices characterization, optical detectors, power devices, and radiation hard devices.